Direct Numerical Simulation of Chemical Selectivity in Homogenous Turbulence

Mitali Chakrabarti, Robert M. Kerr, and James C. Hill
Dept. of Chemical Engineering, Iowa State University, Ames, IA 50011

Direct numerical simulations were used to study chemical selectivity in a series-parallel reaction scheme in a decaying, homogenous turbulent flow, where A, B, R, and S represent chemical species with R the principal product and S the secondary product. These simulations involve solution of the unsteady Navier-Stokes and mass conservation equations by a pseudo-spectral method in a 64^3 wavenumber domain. Reactants A and B were initially spatially segregated, corresponding to a nonpremixed system. The effect of turbulence Reynolds number and other physical parameters on selectivity was determined. Turbulence increases the formation of primary product R over byproduct S compared to the case of no fluid motion, as expected. It was also found that any mechanism promoting homogenization of reactants favors the formation of R, whereas any mechanism sustaining segregation favors the formation of S.

Introduction

Many industrial processes involve chemical reactions in turbulent flow as important steps. Turbulence is often preferred over laminar flow because it enhances heat- and mass-transfer rates. The kinetics of reactions involved in industrial chemical processes are often complex, with multiple steps and many intermediate products. The chlorination of hydrocarbons, the hydration of ethylene oxide, the formation of ethanolamines (Nauman, 1975), and the nitration of aromatic hydrocarbons with nitronium salts (Pfister et al., 1975) are some examples of reaction schemes exhibiting series-parallel behavior. The results of manufacturing the wrong distribution of products are a waste of raw materials and also an increased load on the separation stages to extract the desired product in pure form. Such considerations are also important in air-pollution, propulsion, and combustion problems, which involve a wide range of complex multiple reactions.

Except for combustion studies, the principal fundamental experimental work on turbulent reacting flows with complex chemistry has been carried out by Bourne (1981) who studied a particular series-parallel reaction system—the diazo-coupling reaction, now referred to as Bourne's reaction. Several subsequent experimental studies (Li and Toor, 1986; Mehta and Tarbell, 1987) have made use of Bourne's reaction. It should be noted that in Bourne's reaction, the first reaction is very fast compared to the second. Since most experimental studies were limited to just this particular reaction system, knowledge about turbulent flow with multiple reactions has been extremely limited.

Advances in the power and speed of computers have now made it possible to directly solve the equations for turbulent reacting flows at low to moderate Reynolds numbers. In direct numerical simulations (DNS), the nonlinear dynamical equations are solved with no turbulence modeling and with all time and length scales well-resolved. Direct numerical simulations of three-dimensional chemically reacting homogenous turbulent flow for unmixed reactants in a single step, finite rate reaction have been made by Givi and McMurtry (1988), Leonard and Hill (1988, 1989, 1991) and Mell et al. (1993). Some preliminary investigations on the effect of various physical and chemical parameters for the series-parallel reaction case have been made by Chakrabarti and Hill (1990) for decaying homogenous turbulence and by Gao and O'Brien (1991) for a forced turbulent flow.

In the present study, described in more detail by Chakrabarti (1991), DNS of a series-parallel reaction pair in a decaying, homogenous turbulent flow was used to predict the product distribution in the problem of chemical selectivity and to help explain the interaction of turbulence, mixing,

Correspondence concerning this article should be addressed to M. Chakrabarti who is currently at Altair Engineering Inc., 17333 Federal Drive, Suite 260, Allen Park, MI 48101.
Current address of R. M. Kerr: National Center for Atmospheric Research, P.O. Box 3000, Boulder, CO 80307.

and complex chemistry in this problem. The effect of turbulence, compared to the case with no motion, was studied by examining the variations of product distributions with turbulence intensity and viscosity, that is, by varying the turbulence Reynolds number. The effects of other physical parameters such as Schmidt numbers, diffusivities, reaction rate constants, initial stoichiometric ratios, and initial scalar field conditions were also studied. Comparisons between the single reaction and the series-parallel reaction systems were made to better understand the complexity introduced by a two-step chemical reaction. These results are used in a forthcoming article in which several models are evaluated (Chakrabarti and Hill, 1995).

Background

Series-parallel reactions are among the simplest forms of complex chemistry schemes, and so they are studied in the investigation reported here. A simple model series-parallel reaction scheme for chemical species A, B, R, and S is:

$$A + B \xrightarrow{k_1} R$$

$$R + B \xrightarrow{k_2} S, \tag{1}$$

where R, the intermediate product, will be considered the desired product and S, the undesired product. In the case of a simple single step reaction, reactants A and B react to form the product R. But in our case, A and B first react to form R by the first reaction, B then further reacts with the R formed to produce S. When a substantial amount of R has been formed, both A and R compete for the B present in the system to form either more R or S, respectively. And the outcome of this competition determines the product distribution.

The measure of selectivity used here (X_S) is the ratio of the amount of B that reacts to form byproduct S to the total amount of B reacted (Bourne et al., 1981) and is given by the equation:

$$X_S = \frac{2\bar{C}_S}{\left(2\bar{C}_S + \bar{C}_R\right)}, \tag{2}$$

where $\bar{C}_R$ and $\bar{C}_S$ are the mean concentrations of R and S, respectively.

In a turbulent flow field, vortex stretching and distortion of fluid elements by turbulence causes the concentration gradients of the reactants to increase and increases the area of the interface between them (Patterson, 1985). Turbulent diffusion reduces the scale of segregation to a considerable degree, and molecular diffusion ultimately mixes the two fluids on a molecular level. Thus the rate of mixing is greatly enhanced by turbulence. If more than one reaction occurs simultaneously, then interactions between turbulence enhanced mixing and reaction become very important, since it is recognized that selectivity to specific products is a strong function of mixing rate (Patterson, 1985). That complex reactions are strongly affected by the mixing intensity has been noted by other investigators such as Paul and Treybal (1971) and Cheng and Tookey (1978).

Paul and Treybal (1971) studied the product distribution for a homogenous, liquid phase, series-parallel reaction and found that the reaction rate and/or the product distribution may be influenced by mixing if the course of the reaction is influenced by concentration. Based on laboratory measurements of the yield of the diazo-coupling reactions in a CSTR, Bourne et al. (1978, 1981) observed that the product distribution from fast, series-parallel reactions, depends upon the stoichiometric ratio, the volumetric ratio of the reagent solution, the location of the feed point, the backmixing into the feed pipe, the operating mode of the reactor, the viscosity of the solutions, the type, diameter and rotation speed of the impeller, and the concentrations of the feed solution and concentrations in the tank. They found that secondary product formation can be reduced by one or a combination of the following measures: increasing the agitator input, reducing the solution viscosity, reducing the reaction temperature, avoiding high volume ratios, using dilute reagent solutions, increasing the stoichiometric ratio, and so on. The experimental results were used to validate the mechanistic engulfment-deformation-diffusion model of Baldyga and Bourne (1984). Li and Toor (1986) found that for Bourne's reaction the yield decreases with a decrease in the Reynolds number and with an increase in the ratio of the mixing speed to intrinsic reaction speed, in both the single-jet and the multijet reactors. The data from these experiments was compared with predictions of mechanistic models such as the slab diffusion model (Mao and Toor, 1971). Heeb (1986) carried out experiments with a polymerization reaction. The work was rather inconclusive, however, but led to suggestions of potentially better systems. Mehta and Tarbell (1987) used Bourne's reaction in an unmixed feedstream multijet tubular reactor and observed that the concentration profiles (particularly the S profile) showed large deviations from the perfect mixing limit corresponding to a plug-flow reactor. Mechanistic models such as the three-environment model and four-environment model (Mehta and Tarbell, 1983) use data from these experiments to determine the value of the micromixing parameter for the models (Tarbell and Mehta, 1986).

Problem

The model series-parallel reaction system being studied is Eq. 1, where R is the desired product and S is the undesired product. The reaction rates are second-order with known constant reaction rate coefficients that are of the same order of magnitude for each reaction in order to avoid a set of stiff differential equations. The effective binary Fickian diffusion coefficient and all physical properties are constant. The fluid is incompressible, and the scalar field is passive with respect to the velocity field. The velocity field is a decaying, homogenous turbulent flow field with no mean gradients, and averages (as indicated by overbars) are evaluated as volume averages over the entire domain.

The problem is equivalent to that in which the observer follows the flow in a turbulent plug-flow reactor with the mean velocity, as shown in Figure 1. An initial turbulence level is specified, and then the velocity fluctuations decay in time as viscous dissipation reduces the velocity gradients. The physical space domain for the simulation is a transparent cube with sides of length L ($= 2\pi$), with periodic boundary conditions for all variables and the units used are arbitrary. The

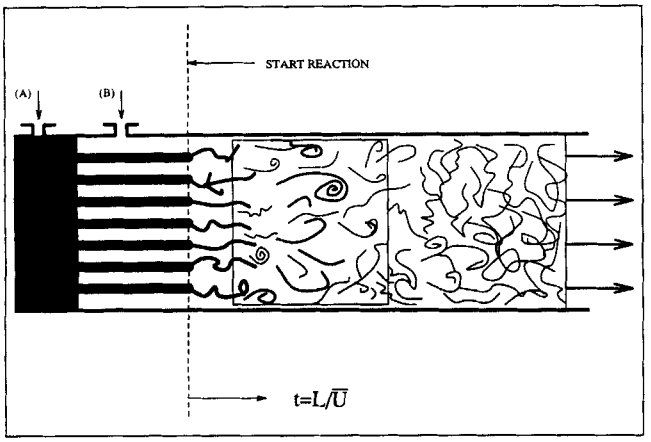

Figure 1. Plug-flow reactor.
Adapted from Hill (1976).

square box in the reactor in Figure 1 is a face of the cube. The relationship between time in the simulations and distance in the plug-flow reactor is, as indicated in Figure 1, $t = L/\bar{U}$, where $\bar{U}$ is the mean velocity in the PFR. Initially, the reactants A and B are spatially segregated, and no products R or S are present. For most simulations, alternating slabs of reactant species are used as initial conditions for concentration values in order to make visualization of the reaction zones easier. Some simulations were done for the case where the scalar field (reactants A and B) is isotropic. Sketches of these initial scalar fields are shown in Figure 2.

The velocity field is governed by the Navier-Stokes equation:

$$\frac{\partial \boldsymbol{u}}{\partial t} + \boldsymbol{u}\cdot\nabla\boldsymbol{u} = -\frac{\nabla p}{\rho} + \nu\nabla^2\boldsymbol{u}, \tag{3}$$

with the incompressibility condition

$$\nabla\cdot\boldsymbol{u} = 0. \tag{4}$$

The concentration C_i of species "i"$= A, B, R, S$ is governed by the mass conservation equation:

$$\frac{\partial C_i}{\partial t} + \boldsymbol{u}\cdot\nabla C_i = D_i\nabla^2 C_i + r_i, \tag{5}$$

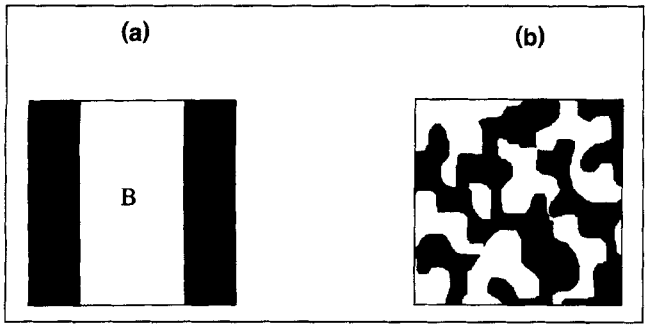

Figure 2. Scalar initial fields.
(a) Slab initial scalar field; (b) blob initial scalar field.

where r_i is the rate expression for the creation of species "i" and D_i is the molecular diffusivity of species "i". The diffusivities of all species are set equal. The governing equations are solved with a pseudo-spectral method using a code adapted from Kerr (1985). The fluid velocity field is represented by the Fourier expansion:

$$\boldsymbol{u}(\boldsymbol{x},t) = \sum_{n=1}^{N} \hat{\boldsymbol{u}}(\boldsymbol{k},t)e^{i\boldsymbol{k}\cdot\boldsymbol{x}}, \tag{6}$$

and the concentration field by:

$$C_i(\boldsymbol{x},t) = \sum_{n=1}^{N} \hat{C}_i(\boldsymbol{k},t)e^{i\boldsymbol{k}\cdot\boldsymbol{x}} \tag{7}$$

for a wavenumber domain of N^3 Fourier modes. The rotational form of the Navier-Stokes equation,

$$\frac{\partial \boldsymbol{u}}{\partial t} = \boldsymbol{u}\times\omega - \nabla\left(\frac{p}{\rho} + \frac{u^2}{2}\right) + \nu\nabla^2\boldsymbol{u}, \tag{8}$$

is used because it conserves kinetic energy in the absence of time-stepping errors and viscous dissipation (Orszag, 1971). The conservative form of the mass conservation equation,

$$\frac{\partial C_i}{\partial t} + \nabla\cdot\boldsymbol{u}C_i = D_i\nabla^2 C_i + r_i, \tag{9}$$

is used, where "i" represents the chemical species A, B, R, or S.

The Fourier components of the dynamical variables are integrated forward in time using a third-order Runge-Kutta algorithm designed to minimize memory requirements. The time integration uses a variable time-step based on a Courant-Friedrichs-Lewy (CFL) stability criterion modified to include the effects of a finite reaction rate. The Courant number is defined as:

$$C = \max\left[\Sigma_i\frac{|u_i|}{\Delta x_i} + k_1\max(C_A,C_B,C_R,C_S)\right]\Delta t, \tag{10}$$

where u_i is fluctuating component of the velocity in the i-direction, Δx_i is the grid-spacing in the i-direction, and the maximum value is evaluated over the entire domain (Leonard, 1989). The nonlinear terms are evaluated in physical space and then transformed back to wavenumber space using fast Fourier transforms (FFT). The pressure term is evaluated in wavenumber space by using the solenoidal property of the velocity field. Partial de-aliasing is accomplished by spherical truncation of wavenumbers outside a spherical shell of radius 8K/9. The initial energy spectrum for the velocity field has been chosen to be "Gaussian" ($ak^4e^{-bk^2}$), "exponential" (ak^3e^{-bk}), or of the form $a(kb)^4/[1+(kb)^2]^3$ (Eq. 3-151, Hinze, 1975) where a and b are given in Table 1. The theoretical and measured (in simulations) values of the integral length scale, Taylor microscale and Kolmogorov microscale for the different spectra are also shown in Table 1. The details of the derivations of the theoretical forms of the length

Table 1. Initial Velocity Field Energy Spectra

Spectrum	$E(k,0)$	a	b	Λ_f	λ_g	η
"X"	$ak^4e^{-bk^2}$	$\frac{16u'^2}{k_0^5}\sqrt{\frac{2}{\pi}}$	$\frac{2}{k_0^2}$	T**: 1.00	T: 0.8	T: 0.07
				M†: 0.99	M: 0.78	M: 0.07
"Y"	ak^3e^{-bk}	$\frac{81}{4}\frac{u'^2}{k_0^4}$	$\frac{3}{k_0}$	T: 0.94	T: 0.6	T: 0.06
				M: 0.82	M: 0.58	M: 0.06
"Z"	$\frac{a(kb)^4}{(1+(kb)^2)^3}$	$\frac{8\sqrt{2}u'^2}{\pi k_0}$	$\frac{\sqrt{2\pi}}{k_0}$	M: 0.94	M: 0.3	M: 0.05

*Derivations for constants a and b and the different length scales are given in Chakrabarti (1991). The peak wave number, k_0 is 2.5 and the cut-off is 32.
**T implies evaluated from theoretical expressions given in Chakrabarti (1991).
†M implies measured from simulations.

scales are given in Chakrabarti (1991). In the present study, the simulations used an initial Gaussian energy spectrum (X), unless otherwise mentioned.

The same initial conditions for the velocity field (the same seed for the random number generator) were used for all runs except for three runs which were done with three different random number seeds. The statistical quantities such as R_λ, $\overline{C_A}$, and $\overline{c_B c_R}$ are almost identical for the three cases and so the calculations presented here are a realistic representative sample. The viscous dissipation spectra and the scalar dissipation spectra were evaluated, and it was found that the simulations were well-resolved. Increasing the Courant number (Eq. 10) corresponds to increasing the time-step, so the computer time for the simulation is reduced but time-stepping errors become significant. Simulations were done with Courant numbers of 1.0 and 1.5 and the statistical quantities were almost identical for the two cases. The higher Courant number ($=1.5$) was chosen for the simulations so as to reduce the computer time needed.

Two types of initial scalar fields, shown in Figure 2, are used in this study. One corresponds to the slab or striped case where the initial concentration distribution of reactant species is similar to that used by Leonard and Hill (1989), in which the initial scalar field corresponds to spatially segregated slabs of reactants parallel to the x plane, such that B lies in the center half of the domain and A lies to the sides.

The other type of initial scalar field corresponds to the blob or prestirred case, where the scalar field is approximately isotropic. The scalar field is preconditioned to create realistic spatial structures for the concentrations of A and B. For this case, both the velocity and scalar fields are preprocessed. An initial energy spectrum of the form

$$E(k,0) \propto \frac{(k\Lambda_f)^4}{\left[1+(k\Lambda_f)^2\right]^3} \tag{11}$$

was specified for the presimulation. To generate a statistically isotropic scalar field, the scalar field is preconditioned as follows. The Fourier coefficients of a Gaussian random variable ϕ are scaled to fit a prescribed concentration spectrum of the form:

$$E_\phi(k,0) \propto \frac{(k\Lambda_f)^3}{\left[1+(k\Lambda_f)^2\right]^2}. \tag{12}$$

The function ϕ is allowed to convect and diffuse for some time (until $t = 0.4$, that is, about one-half of an eddy turnover time) while the velocity field is being pretreated. In regions where ϕ is positive, the concentration of A is assigned a value of 2 and in regions where ϕ is negative, B is assigned the value 2. The Fourier transform of this concentration field is used as initial values for the scalar field. Diffusive damping of the initial conditions ($Dt^* = 0.02$) was used at the beginning of the simulation for both initial scalar fields to avoid negative concentrations produced by Gibb's ringing.

Simulations in this study were carried out in decaying isotropic turbulence on a grid of 64^3 Fourier modes. The calculations were done on the Cray X/MP and Cray Y/MP at the National Center for Supercomputer Applications, IL and on the Cray Y/MP at the Ohio Supercomputer Center. The computational or "cpu" time per time-step for the simulations was about 12 s on the Cray Y/MP, and a typical simulation needed about 250 time-steps.

The turbulence Reynolds number (R_λ) and other physical parameters were varied for the different calculations performed. The turbulence Reynolds number R_λ is a measure of turbulence and is defined as $u'\lambda/\nu$, where u' is the turbulence intensity, λ is the Taylor microscale for the velocity field, and ν is the viscosity. The velocity field description is given in Table 1, where R_λ refers to initial velocity fields. Decay of the velocity field proceeds as given by Leonard and Hill (1991). Initial conditions and parameters for the simulations along with the corresponding labels for the different cases are given in Table 2.

Results and Discussion

The behavior of the single reaction system when compared to the case with complex chemistry is significantly different. Figures 3a and 3b show the time evolution of the reactants A and B and products R and S for the cases of single and multiple reactions in a homogeneous decaying turbulent flow field for conditions of case K and case A, respectively. The decay of B is faster in the case of the series-parallel reaction,

Table 2. Initial Conditions for the Simulations*

Case	Parameters						Dimensionless Groups			
	ν	D	k_1	k_2	u'	C_{A0}/C_{B0}	R_λ	Sc	Da_1	Da_2
A	0.025	0.036	5	1	0.96	1	29.93	0.7	5.16	1.03
B	0.025	0.036	5	1	1.06	1	33.12	0.7	4.67	0.93
C	0.025	0.036	5	1	1.45	1	45.07	0.7	3.41	0.68
D	0.04	0.057	5	1	0.96	1	18.70	0.7	5.16	1.03
E	0.10	0.143	5	1	0.96	1	7.48	0.7	5.16	1.03
F	0.04	0.036	5	1	0.96	1	18.70	1.12	5.16	1.03
G	0.10	0.036	5	1	0.96	1	7.48	2.8	5.16	1.03
H	0.025	0.25	5	1	0.96	1	29.93	0.1	5.16	1.03
I	0.025	0.062	5	1	0.96	1	29.93	0.4	5.16	1.03
J	0.025	0.025	5	1	0.96	1	29.93	1.0	5.16	1.03
K	0.025	0.036	5	0	0.96	1	29.93	0.7	5.16	0
L	0.025	0.036	5	2.5	0.96	1	29.93	0.7	5.16	2.58
M	0.025	0.036	5	5	0.96	1	29.93	0.7	5.16	5.16
N	0.025	0.036	1	2	0.96	1	29.93	0.7	1.03	2.06
O	0.025	0.036	2.5	5	0.96	1	29.93	0.7	2.58	5.16
P	0.04	0.036	5	1	0.96	0.67	18.70	0.7	4.22	0.84
Q	0.04	0.036	5	1	0.96	0.9	18.70	0.7	4.89	0.98
R	0.04	0.036	5	1	0.96	1.2	18.70	0.7	5.65	1.13
S	0.04	0.036	5	1	0.96	1.5	18.70	0.7	6.32	1.26
T	-	0.036	5	1	0.0	1.0	0.0	-	-	-

*Note: The values of R_λ, Da_1 and Da_2 correspond to an initial Gaussian energy spectrum, "X". For spectrum "Y", R_λ should be multiplied by 0.74 and Da_1 and Da_2 should be multiplied by 0.83. For spectrum "Z", R_λ should be multiplied by 0.38 and Da_1 and Da_2 should be multiplied by 0.95.

because B is being consumed by both reactions. The production of R keeps increasing till A and B are exhausted in the case of a single reaction, whereas with a series-parallel reaction scheme R is formed by one reaction and is consumed by the second. The system reaches an asymptotic state once B is fully consumed. The evolution of R and S for the blob case is discussed later.

DNS results have been analyzed for initial slab and isotropic (blob) scalar fields. The correlation coefficient for A and B is defined as $\gamma_{AB}=\overline{c_A c_B}/(c'_A c'_B)$ and that for B and R as $\gamma_{BR}=\overline{c_B c_R}/(c'_B c'_R)$. These are shown in Figure 4 for the single reaction case and the series-parallel reaction case for a slab initial scalar field. The intensity of segregation I_s for A and B, defined as $-\overline{c_A c_B}/(\overline{C_A}\,\overline{C_B})$, and I_s for B and R, defined as $-\overline{c_B c_R}/(\overline{C_B}\,\overline{C_R})$, were determined and the time evolution of I_s for A and B, and I_s for B and R for the slab and blob case for the series-parallel reaction is shown in Figure 5. The time evolution of I_s for A and B and I_s for B and R for the single reaction case and a slab initial scalar field is also shown in Figure 5. The definition of I_s used here is one defined for reacting systems (Danckwerts, 1952; Hill, 1976). This differs from definitions commonly used (for example, that

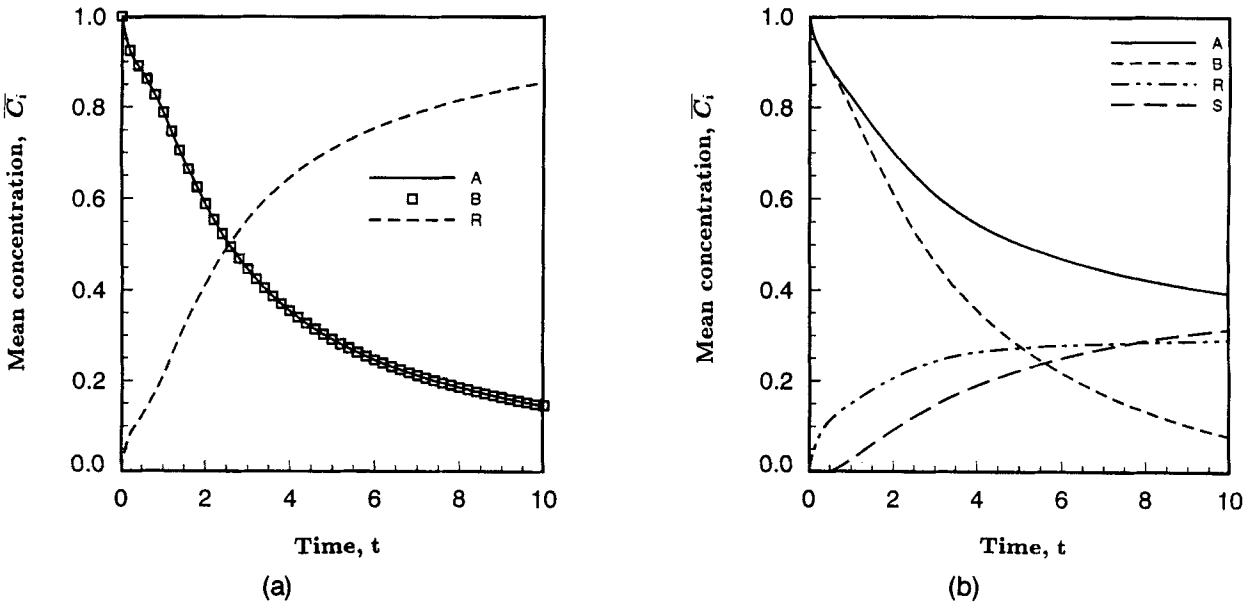

Figure 3. Time history of reactants and products for case A and an initial slab scalar field.

(a) Single reaction; (b) series-parallel reaction.

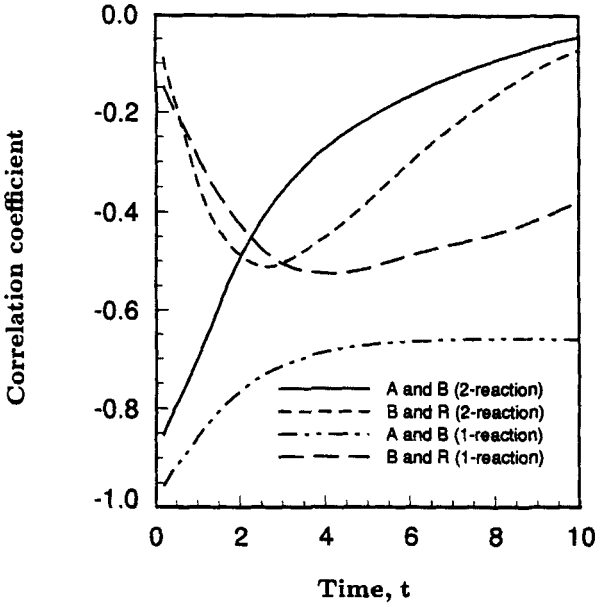

Figure 4. Correlation coefficients γ_{AB} and γ_{BR} for single-step (case K) vs. two-step (case A) reactions for slab initial conditions of the scalar field.

used by Gao and O'Brien, 1991) in modeling reacting systems with a conserved scalar. The values obtained for I_s for A and B imply a very high degree of segregation. This is expected, since initially segregated reactants were used. The values of I_s for B and R suggest imperfect mixing, but also suggest that B and R are more mixed than A and B are. These conditions are different from those used by Gao and O'Brien

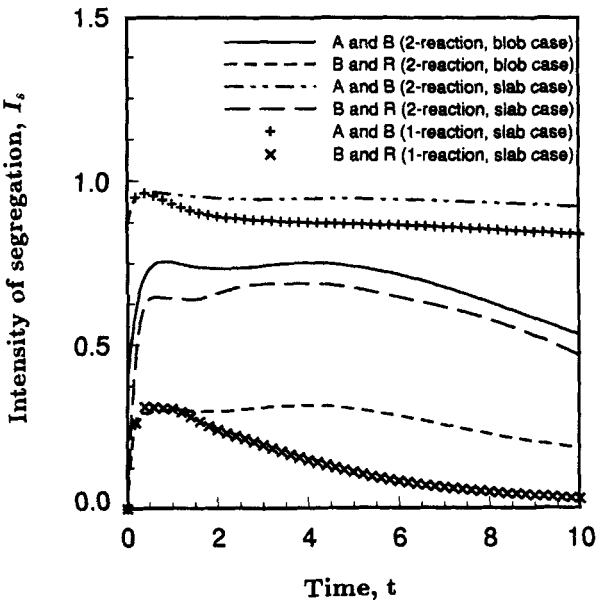

Figure 5. Intensity of segregation I_s for case A for slab and blob initial scalar fields vs. case K for a slab initial scalar field.

I_s for A and B is $-\overline{c_A c_B}/\overline{C_A C_B}$, I_s for B and R is $-\overline{c_B c_R}/\overline{C_B C_R}$.

Table 3. Initial Damköhler Numbers for the Slab and Blob Scalar Fields for Case A

Initial Scalar Field	First kind, Da_I		Second kind, Da_{II}	
	$\frac{k_1 C_{A0} \Lambda_f}{u'}$	$\frac{k_2 C_{A0} \Lambda_f}{u'}$	$\frac{k_1 C_{A0} \lambda_g^2}{D}$	$\frac{k_2 C_{A0} \lambda_g^2}{D}$
Slab Case	5.16	1.03	84.5	16.9
Blob Case	5.96	0.945	79.3	15.86

(1990) who had zero initial correlation for the scalar fields and a forced turbulent flow field. The values of I_s obtained from the simulations also show that the slab initial scalar field corresponds to a more segregated scalar field compared with the blob initial scalar field, again as expected. For conditions of case A, the first and second Damköhler numbers for the two reactions were evaluated for both slab and blob initial scalar fields and are given in Table 3. The first reaction can be said to be moderately fast while the second reaction is slow.

Next, we will discuss some local reaction rates that bear on the behavior discussed earlier and also examine the effect of various physical parameters on product distribution and selectivity.

Structure of reaction zones

A point to note about series-parallel reactions is that there are two reaction zones, one for each reaction, although there is considerable overlap. In the absence of a velocity field, distribution of products for the complex chemistry case will depend on the initial distribution of reactants. If A and B have the same initial concentration distributions with the same peak values but merely spatially displaced, or in other words, if A and B are initially anticorrelated, the peak value of the generation rate of R would initially occur in the region of overlap of the two distributions and R would be distributed symmetrically about the peak. The distribution of R will depend on the details of the spatial distribution of A and B. The generation rate of S resulting from the reaction of B and R will be greatest inside the B rich region. If A is given by $A_0 e^{[-\alpha(x+x_0)^2]}$ and B is given by $B_0 e^{[-\alpha(x-x_0)^2]}$, then δR will be $k_1 A_0 B_0 e^{[-2\alpha(x^2+x_0^2)]}\delta t$, where δR is the incremental amount of R produced in time δt. The actual value of R after a short interval of time can be found by solving the one-dimensional diffusion equation. The distribution of R would be similar in form to the distribution of the generation rate of R except for the spread caused by diffusion. The second reaction starts only after some R has formed. Also, some B has already been consumed. The generation rate of S in the initial period will be given by $\delta S \alpha R_1 B_1$, where R_1 and B_1 are the values of R and B, respectively, at time δt. Since the reaction system is closed, that is, A and B are not replenished, the result of the reaction is to cause a reduction in the total values of A and B. The reductions are initially localized. The effect of diffusion would be to cause a redistribution of A and B and can be computed by solving the diffusion equation. The consumption rate of B is higher than A because B takes part in two reactions. The peaks of the distribution of R and S are towards the A-rich region and B-rich region, respectively. The above simple explanation is for the

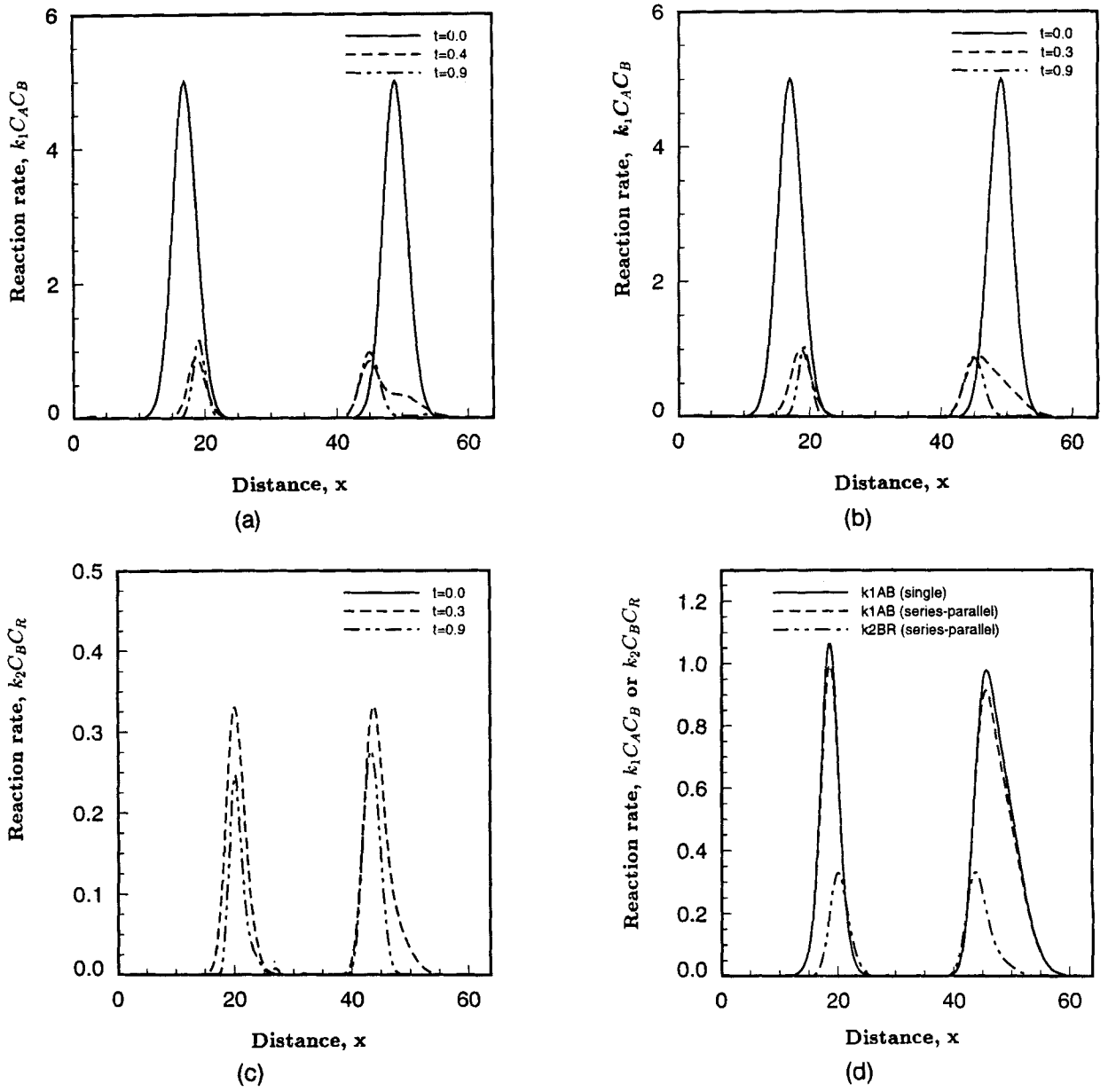

Figure 6. Reaction rate profiles along the line $y = z = 0$ for slab initial conditions.

(a) $k_1C_AC_B$ for Case K (single reaction); (b) $k_1C_AC_B$ for Case A (two-step reaction); (c) $k_2C_BC_R$ for Case A (two-step reaction); (d) comparison of (a), (b), (c) at $t = 3.0$.

case of no motion, but we expect qualitatively similar behavior in the actual system.

In the presence of a turbulent velocity field, the time evolution and spatial variation of the reaction zone depends on the velocity field, as well as on reaction and diffusion. Figure 6a shows the spatial variation of the reaction rate $k_1C_AC_B$ at three different times, for the case of a single reaction. The two peaks in the profile of $k_1C_AC_B$ represent the two spatial locations of the reaction zone, for the first reaction. Figures 6b and 6c show the spatial variation of reaction rates $k_1C_AC_B$ and $k_2C_BC_R$ respectively, for the case of a series-parallel reaction scheme, also at three different time levels. The value of $k_1C_AC_B$ is the highest initially, and the peak falls as A and B are consumed by the reactions. The second reaction rate $k_2C_BC_R$ is zero initially, because there is no R in the system. Then as R forms, the reaction rate increases but again decreases with time. The reaction rates ($k_1C_AC_B$ and $k_2C_BC_R$) for the multiple reaction case and the reaction rate ($k_1C_AC_B$) for the single reaction case, all at one time, are shown in Figure 6d. This figure shows that the reaction zone for the first reaction in the multiple reaction case almost coincides with the reaction zone for the single reaction. The reaction zones for the two reactions do not coincide, however, in the multiple reaction case. The reaction zone for the second reaction appears to have migrated towards the B-rich region because the second reaction depends on the presence of B in the system and not on A. The reaction zone for the first reaction does not migrate with respect to the reaction zone for the single reaction because the first reaction depends on the presence of both A and B.

Effect of physical parameters

It has been noted by Levenspiel (1972) that for the case of a very fast series-parallel reaction, it is important to achieve homogeneity in A and R in order to favor the formation of the intermediate R. Previous simulations have confirmed the general validity of this observation (Chakrabarti and Hill, 1990). In fact, the effect of turbulence and other physical parameters such as viscosity, Schmidt number, diffusivity, reaction rate constants, initial stoichiometric ratio and initial conditions on product distribution may be explained very simply: any mechanism sustaining segregation of reactants depresses formation of R, whereas any mechanism causing homogenization (mixing) depresses formation of S. The literature on series-parallel reactions also supports the thesis that segregation depresses the formation of intermediate R (Levenspiel, 1972; Bourne and Toor, 1977).

For the series-parallel reaction, that is, Eq. 1, the ratio of the rates of the two reactions is given as:

$$\frac{\overline{r_R}}{\overline{r_S}} = \frac{k_1(\overline{C_A C_B} + \overline{c_A c_B}) - k_2(\overline{C_B C_R} + \overline{c_B c_R})}{k_2(\overline{C_B C_R} + \overline{c_B c_R})}. \qquad (13)$$

Since c_i are the fluctuations due to imperfect mixing, $\overline{c_B c_R}$ is a measure of the imperfections in mixing. Bourne and Toor (1977) have shown that for separate feeds, imperfect mixing lowers the value of r_R/r_S. According to Levenspiel (1972), if there is any nonhomogeneity in A and R, the formation of S is favored, since the reaction zones (zones between regions of high A concentration and high B concentration) contain higher concentrations of R than the surrounding regions, and there is thus a steep concentration gradient and R mixes and reacts with B to form S. But if A and R are spatially homogenous or are present together, they can compete with each other for the B present and produce more R or S. If they are not spatially homogenous, then R reacts with B to form S. These situations are comparable to the case where B is added slowly to a mixture of A and to the case where A is added slowly to a mixture of B, respectively, as described by Levenspiel (1972). Thus, segregation of reactants favors formation of S, whereas homogenization favors formation of R. A more detailed discussion on the subject is available in Chakrabarti (1991).

Table 4. Effect of Initial Turbulence Reynolds Number on Selectivity at $t = 10$, for $Sc = 0.7$ and Slab Initial Condition

Case*	u'	ν	R_λ	X_S
T	0	-	0	0.740
E	0.96	0.1	7.48	0.637
D	0.96	0.04	18.70	0.638
A	0.96	0.025	29.93	0.631
B	1.06	0.025	33.12	0.618
C	1.45	0.025	45.07	0.577

*Corresponding to Table 2.

Effect of Turbulence Reynolds Number. The presence of turbulence has a marked effect on product distribution and thus on selectivity. Compared to the case with no velocity, it is found that in a turbulent flow field, the mean values of A and B decrease faster, whereas the mean values of R and S increase faster initially, leading to higher conversions. Thus the presence of turbulence favors formation of the desired product R over undesired product S. The effect of turbulence Reynolds number R_λ $(= u'\lambda/\nu)$ was determined by varying the turbulence level and by varying the viscosity, keeping the length scale constant.

Figure 7 and Table 4 show that a lower value of X_S is achieved in the presence of turbulence and that, as the turbulence intensity is increased (that is, R_λ is increased), the selectivity X_S decreases. Thus a high level of turbulence produces a better yield of the desired product than does a lower level. Figure 8 shows that a lower value of viscosity, or in other words, a higher value of R_λ, favors formation of desired product R over undesired product S. Also Table 5 shows that the asymptotic value of X_S increases as viscosity increases. These observations support Bourne's hypothesis that

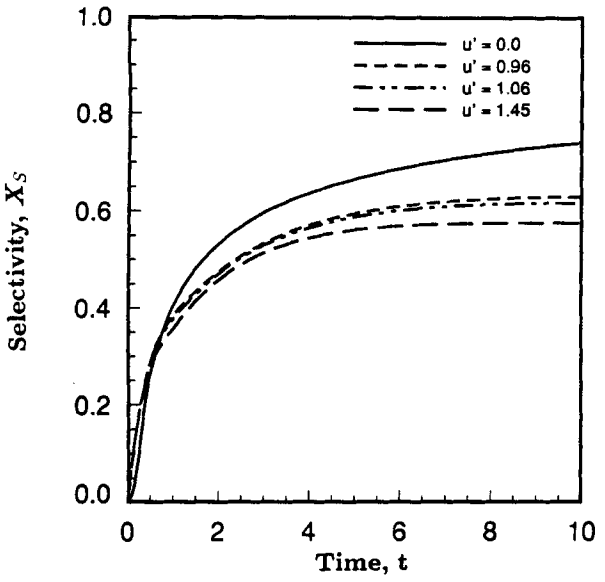

Figure 7. Effect of turbulence intensity on selectivity: cases A, B and C for a slab initial scalar field.

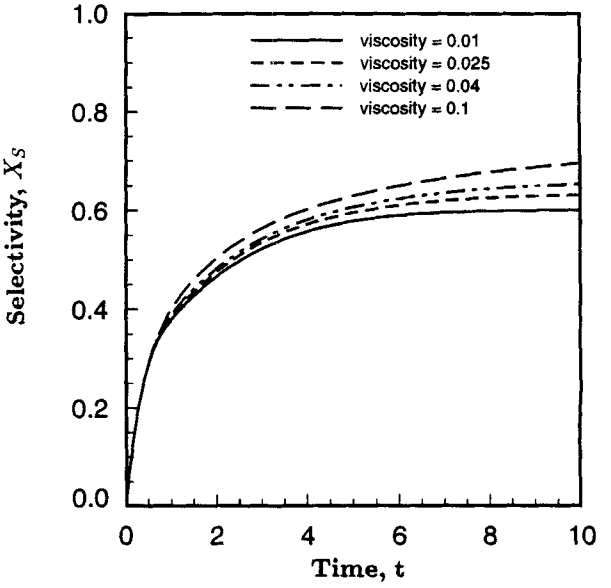

Figure 8. Effect of viscosity on selectivity: cases A, F and G for a slab initial scalar field.

Table 5. Effect of Viscosity on Selectivity at $t = 10$ for a Slab Initial Scalar Field

Case*	ν	Sc	R_λ	X_S
A	0.025	0.7	29.93	0.631
F	0.04	1.12	18.70	0.652
G	0.1	2.8	7.48	0.695

*Corresponding to Table 2.

a reduction of solution viscosity reduces the formation of secondary product S (Bourne et al., 1978; Angst et al., 1982).

Physically, as the turbulence intensity u' increases, that is, as R_λ increases, there is more stretching and distortion of fluid elements and consequently more folding of isoscalar surfaces. As a result, the reaction surface area increases and concentration gradients are steepened, leading to enhanced mixing. Thus transport is enhanced and improved local homogeneity is achieved. As the viscosity is decreased, the flow structure is more detailed, with smaller scales present. The sizes of small-scale structures in the velocity field decrease, and since the scalars are transported with the velocity field, there is also a decrease in the size of the scalar field structure. Figure 9 shows that the scalar microscale, which is a

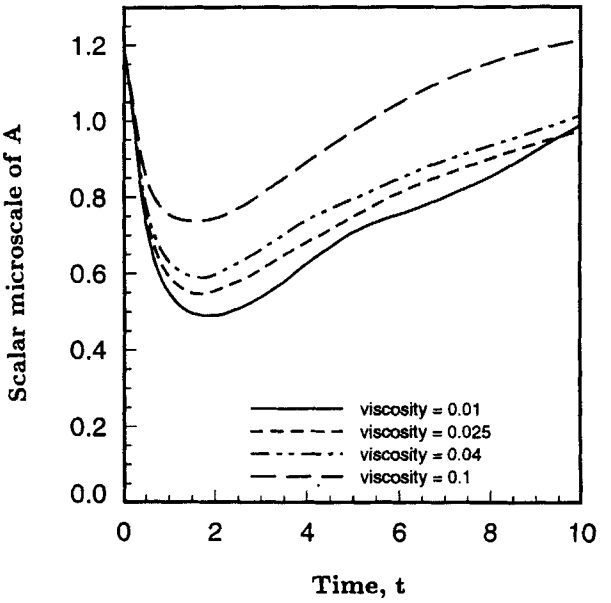

Figure 9. Effect of viscosity on scalar microscale: cases A, F and G for a slab initial scalar field.

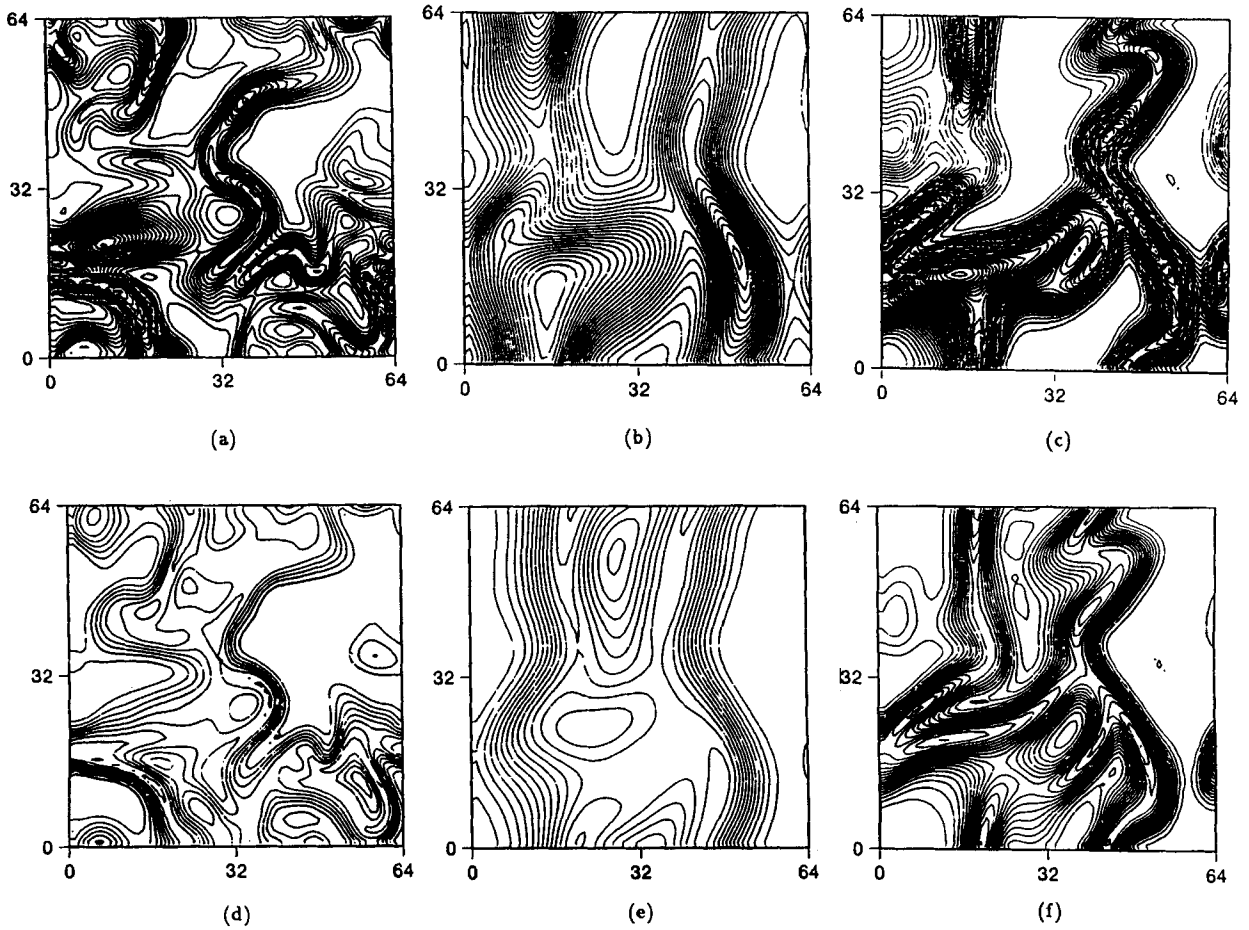

Figure 10. Contours of reaction rate in the plane $z = 0$ at $t = 3.0$ for different viscosities and Schmidt numbers for a slab initial scalar field.

(a) $k_1C_AC_B$ for case A; (b) $k_1C_AC_B$ for case E; (c) $k_1C_AC_B$ for case G; (d) $k_2C_BC_R$ for case A; (e) $k_2C_BC_R$ for case E; (f) $k_2C_BC_R$ for case G.

Table 6. Effect of Schmidt Number on Selectivity at $t = 10$ for a Slab Initial Scalar Field

Case*	ν	D	Sc	R_λ	X_S
H	0.025	0.25	0.1	29.93	0.565
I	0.025	0.062	0.4	29.93	0.616
A	0.025	0.036	0.7	29.93	0.631
J	0.025	0.025	1.0	29.93	0.639
F	0.04	0.036	1.12	18.70	0.652
G	0.1	0.036	2.8	7.48	0.695

*Corresponding to Table 2.

measure of the size of structures in the scalar field, decreases as viscosity is decreased. The isoscalar surface is wrinkled as a result of the small-scale structures in the scalar field, and thus the rate of diffusion of the smaller scales is increased, leading to enhanced transport rates and increased homogenization of the smaller scales. So, an increase in turbulence Reynolds number caused by either an increase of turbulence intensity or by a decrease of viscosity enhances homogeneity and favors the formation of R over the formation of S.

The effect of changes in viscosity on the reaction rates $k_1C_AC_B$ and $k_2C_BC_R$ is shown in Figure 10. Figures 10a and 10b show contour plots of the reaction rate $k_1C_AC_B$ for two different values of viscosity, and Figures 10d and 10e show contour plots of $k_2C_BC_R$ for two different values of viscosity. Figures 10a and 10d, which correspond to a lower value of viscosity and thus a higher value of R_λ compared to Figures 10b and 10e, show finer scale structure. When the viscosity is high, small-scale structures are dissipated more quickly, and hence fewer of those are present than in the case for which the viscosity is low and more scales are present. Thus a lower value of the viscosity produces more detail in the scalar field. Simulations show that the effect of viscosity is the same for both slab and blob initial scalar fields.

Effect of Schmidt Number. The Schmidt number (Sc) is the ratio of viscosity (ν) to diffusivity (D), and thus the effect of Schmidt number on selectivity (keeping ν constant) is essentially the effect of diffusivity on selectivity; a low value of Schmidt number reflects a high value of diffusivity. It is observed from Table 6 that X_S decreases with a decrease in the value of the Schmidt number, which means if diffusivity is increased, more R is formed compared to S.

An increase of diffusivity directly decreases the size of the scalar field structure. Figures 10b and 10c show contour plots of the reaction rate $k_1C_AC_B$ for two different values of Sc whereas Figures 10e and 10f show contour plots of $k_2C_BC_R$. As Sc is decreased, D is increased, there is more transport, hence more homogeneity, and the first reaction is favored over the second.

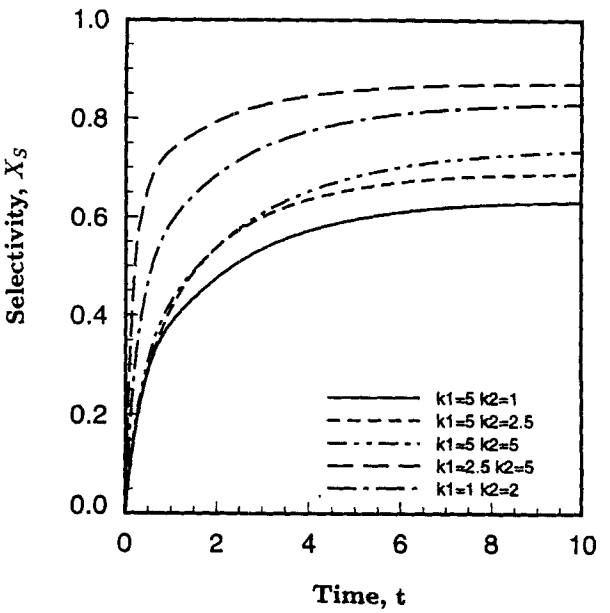

Figure 11. Effect of rate constants on selectivity: cases A, L, M, N and O and a slab initial scalar field.

Coupled Effect of Viscosity and Diffusivity. When the viscosity is decreased for constant Schmidt number, the diffusivity is also decreased. Whereas the effect of a decrease in ν is to decrease X_S, the effect of a decrease in D is to increase X_S. As a result of these competing effects, the selectivity X_S remains relatively unchanged. This effect was observed for different initial energy spectra and is shown in Table 7.

Effect of Rate Constants. As the ratio of the rate constants k_1/k_2 is increased, the formation of both R and S is increased, but the formation of R is favored over the formation of S. That observation is reflected in the decrease in the value of X_S with an increase in the ratio of the rate constants, as is shown in Figure 11 and Table 8.

When $k_1 > k_2$ or $Da_1 > Da_2$,

where

$$Da_1 = k_1\sqrt{C_{AO}C_{B0}}\,\Lambda_f/u'$$

and

$$Da_2 = k_2\sqrt{C_{A0}C_{B0}}\,\Lambda_f/u',$$

Table 7. Coupled Effect of ν and D on Selectivity at $t = 3$ and 10 for a Slab Initial Scalar Field and for Different Initial Energy Spectra

				X_S for Different Initial Energy Spectra					
				"X"		"Y"		"Z"	
Case*	ν	D	R_λ	$t = 3$	$t = 10$	$t = 3$	$t = 10$	$t = 3$	$t = 10$
A	0.025	0.036	29.93	0.535	0.631	0.544	0.660	0.559	0.682
D	0.04	0.057	18.70	0.543	0.638	0.554	0.663	0.568	0.683
E	0.1	0.143	7.48	0.563	0.637	0.572	0.649	0.583	0.667

*Corresponding to Table 2.

Table 8. Effect of Rate Constants on Selectivity at $t = 10$ for a Slab Initial Scalar Field

Case*	k_1	k_2	k_1/k_2	X_S
K	5	0	-	-
O	2.5	5	0.5	0.829
N	1	2	0.5	0.870
M	5	5	1	0.733
L	5	2.5	2	0.688
A	5	1	5	0.630

*Corresponding to Table 2.

Table 9. Effect of Initial Stoichiometric Ratio on Selectivity at $t=10$ for a Slab Initial Scalar Field for $R_\lambda=18.7$, $Sc=0.7$

Case*	P	Q	D	R	S
$\overline{C_{A0}}/\overline{C_{B0}}$	0.67	0.90	1.0	1.2	1.5
X_S	0.753	0.656	0.638	0.617	0.607

*Corresponding to Table 2.

as defined by Gao and O'Brien (1991) for the series-parallel reaction, the first reaction proceeds faster than the second reaction. Thus the initial formation of R by the first reaction is favored. Since both R and A compete for the available B, whether R or S will be preferentially formed depends on the relative rates of the two reactions. As k_1/k_2 increases, the rate of the first reaction increases relative to the second, and thus the formation of R is favored over the formation of S, leading to a decrease in the value of X_S. But for a given pair of reactions, the ratio k_1/k_2 is almost constant and can only be varied slightly by changing the temperature of operation. Another interesting observation is the fact that X_S depends on the absolute values of k_1 and k_2. As Figure 11 shows, X_S increases as k_1 increases for the same k_1/k_2 ratio. Our results are in agreement with the findings of Gao and O'Brien (1991) that for the case of $Da_1 > Da_2$, the formation of S depends upon Da_2, whereas for the case of $Da_1 < Da_2$, Da_1 is the determining factor. The time evolution of the mean concentrations of A, B, R and S for $Da_1 > Da_2$ and for $Da_1 < Da_2$ is shown in Figure 3b and Figure 12, respectively. The figures illustrate that whereas R is rich for $Da_1 > Da_2$, comparatively less R is present when $Da_1 < Da_2$. This has also been observed by Gao and O'Brien (1991). However, the simulations of Gao and O'Brien (1991) are for a forced turbulent flow and zero initial correlation for the scalar fields. The case where $k_1 < k_2$ becomes important is when the second reaction is the desirable reaction and S is the primary product.

Effect of Stoichiometric Ratio. The initial stoichiometric amount of B in the case of series-parallel reactions can be interpreted as either the amount of B needed for the first reaction or as the amount of B needed for both the first and second reaction. The stoichiometric ratio is defined as $\overline{C_{A0}}/\overline{C_{B0}}$ for the first interpretation and $2\overline{C_{A0}}/\overline{C_{B0}}$ for the second interpretation. $\overline{C_{A0}}/\overline{C_{B0}} = 0.5$ is the minimum initial concentration ratio required for the second reaction to go to completion. Simulations show that as the value of the initial stoichiometric ratio ($\overline{C_{A0}}/\overline{C_{B0}}$) is increased, the asymptotic value of X_S decreases, as is evident from Table 9. Also, X_S increases to its asymptotic value faster for higher values of $\overline{C_{A0}}/\overline{C_{B0}}$, as shown in Figure 13.

If the initial stoichiometric ratio ($\overline{C_{A0}}/\overline{C_{B0}}$) is greater than 0.5, B is the limiting reagent, and R is not fully converted to S as the reactions run to completion, since B becomes exhausted. Thus, to form significant amounts of R, the initial stoichiometric ratio ($\overline{C_{A0}}/\overline{C_{B0}}$) should be greater than 0.5 (such as around unity). If initial stoichiometric ratios greatly in excess of 1 are used, very little S is formed. Though X_S is very low in such cases, the price is a low conversion of A and hence a waste of raw materials or increased separation costs.

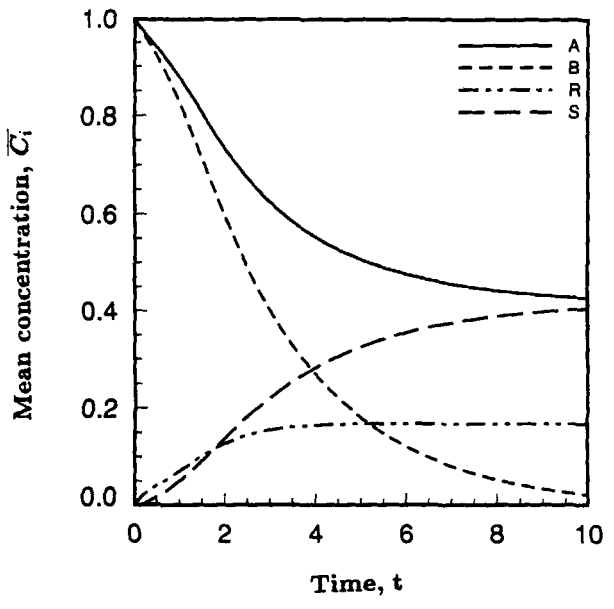

Figure 12. Time history of reactants and products for case O, $k_1/k_2 = 0.5$ and a slab initial scalar field.

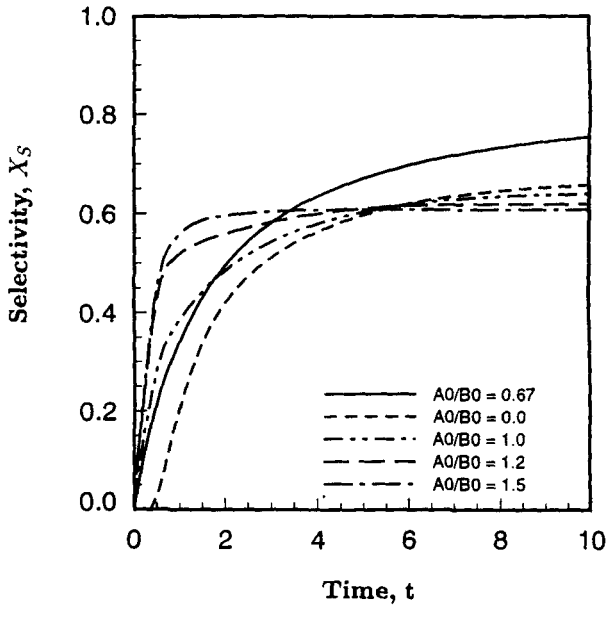

Figure 13. Effect of nonstoichiometry on selectivity: cases P, Q, D, R and S and a slab initial scalar field.

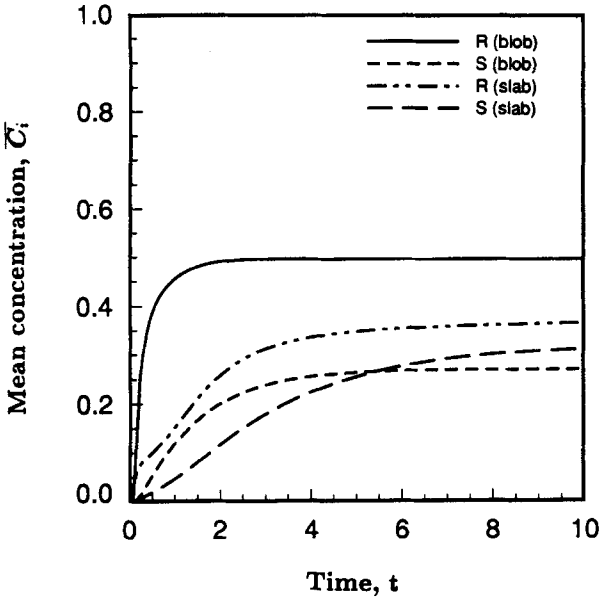

Figure 14. Effect of initial conditions on the evolution of *R* and *S*: case A with slab (1-d) and blob (3-d) initial distribution of reactants *A* and *B*.

Increasing the initial stoichiometric ratio implies decreasing the amount of B available for reaction, so that B is depleted earlier. Thus more R is formed and X_S reaches its asymptotic value faster. Experimental results from a CSTR show that product distribution is not highly sensitive to stoichiometric ratio when this ratio is around 1 (Bourne, 1982).

Effect of Initial Conditions. The above results on the effects of turbulence Reynolds number (R_λ), viscosity, diffusivity and Schmidt number on selectivity show that homogenization of reactants is the key factor controlling the amount of R and S produced and consequently in determining X_S. These results were all for the slab initial scalar field. A study of the effect of different initial fields for the reactants, however, further supports the above observation.

Figure 14 shows that the amount of R produced is considerably higher for the isotropic initial scalar field than for the

Table 10. Effect of Initial Scalar Field on Selectivity

Initial Scalar Field	Selectivity, X_S		
	$t = 0.6$	$t = 3.0$	$t = 10.0$
Slab	0.315	0.535	0.630
Blob	0.250	0.491	0.521

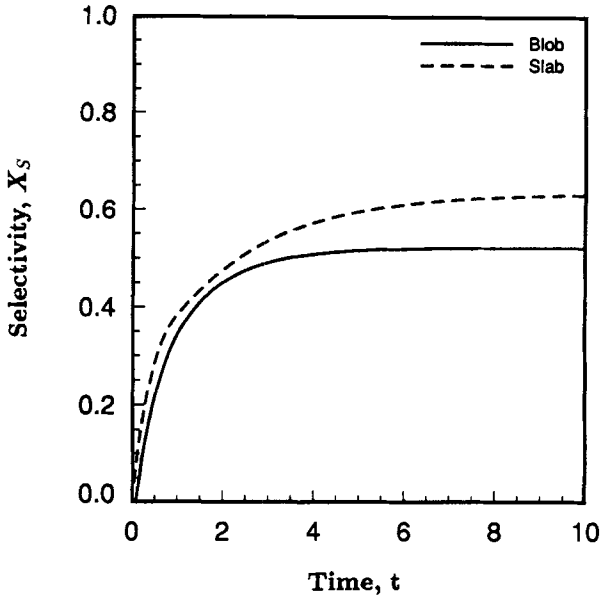

Figure 15. Effect of initial conditions on selectivity: case A with slab (1-d) and blob (3-d) initial distribution of reactants *A* and *B*.

slab initial field. Consequently, a lower value of X_S is obtained for the blob case compared to the slab case as is shown in Table 10 and Figure 15. For the slab case, transport is initially one-dimensional until the other concentration scales parallel to the slab develop (Leonard and Hill, 1991). For the blob or prestirred case, the initial scalar field is a three-dimensional field, with A and B distributed randomly in all three directions. So the reactants A and B are better mixed

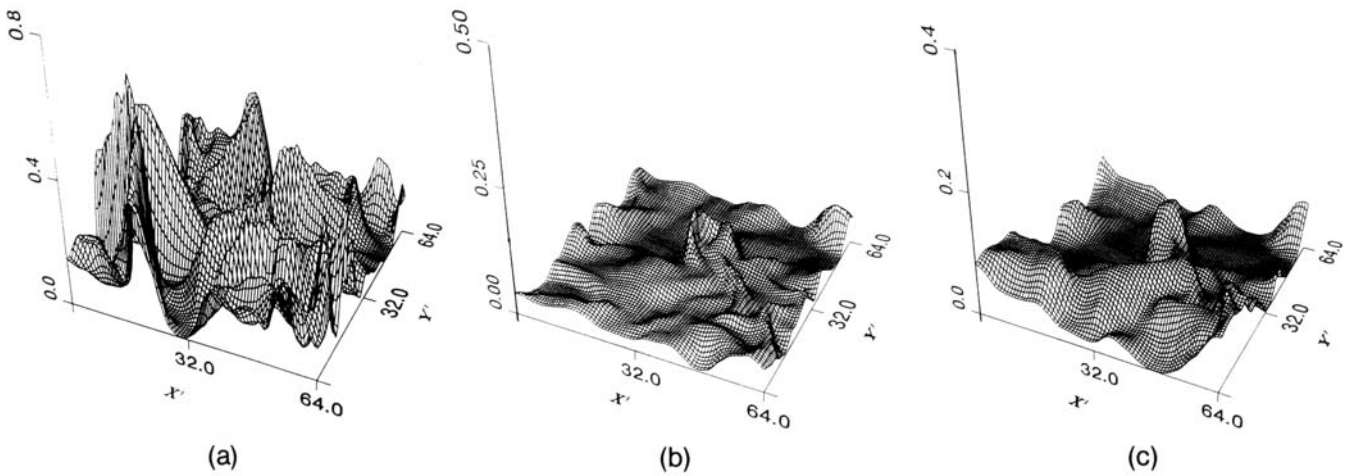

Figure 16. Perspective plots of reaction rates in the plane $z = 0$, at $t = 3.0$ for case A.

(a) $k_1C_AC_B$ for a slab initial field; (b) $k_1C_AC_B$ for a blob initial field; (c) $k_2C_BC_R$ for a blob initial field.

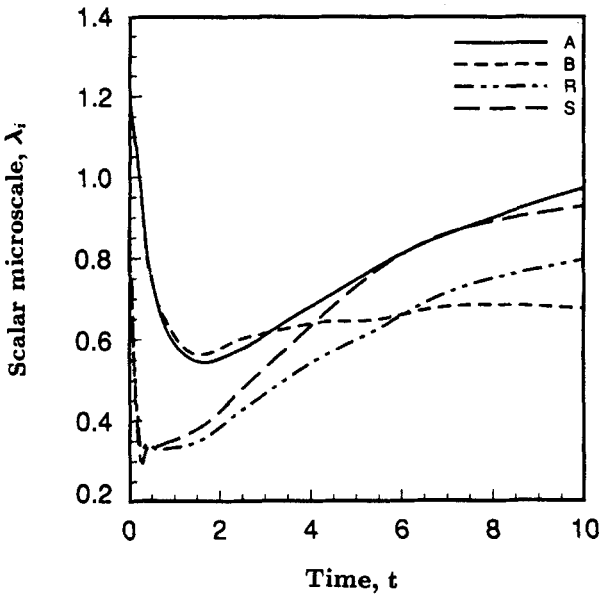

Figure 17. Evolution of scalar concentration microscales for case A and a slab initial scalar field.

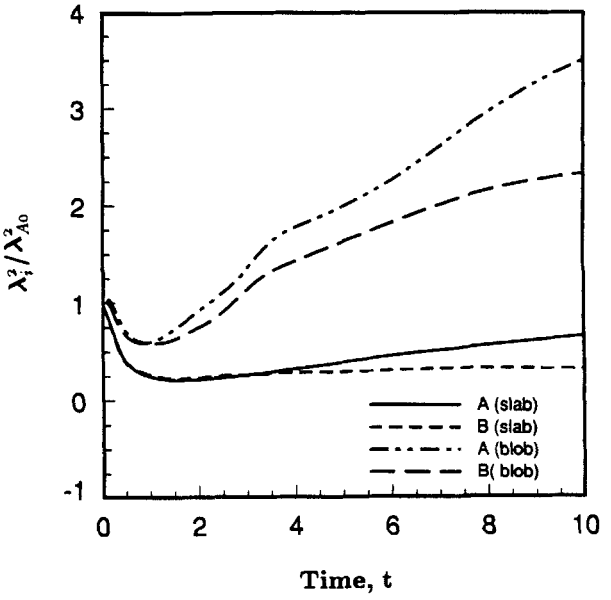

Figure 19. Square of scalar concentration microscales for case A for isotropic (blob) vs. anisotropic (slab) initial scalar fields.

in a macroscopic sense, and the reaction surfaces are more extensive compared to the slab case. The initial integral length scale for the scalar field is 0.51 for the blob case and 1.2 for the slab case, indicating better transport and hence more homogeneity for the blob case. Because of homogeneity in A and R, both A and R can compete for B, and as previously explained, the formation of R is favored over the formation of S. Figures 16a and 16b show perspective plots of the reaction rates $k_1C_AC_B$ for a slab and blob scalar field respectively. Figure 16c shows the perspective plot of the reaction rate $k_2C_BC_R$ for a blob scalar field. Since there is more homogenization with an initially isotropic scalar field, the perspective plot Figure 16b shows smoother contours compared to the contours in Figure 16a which is for an initial slab scalar field.

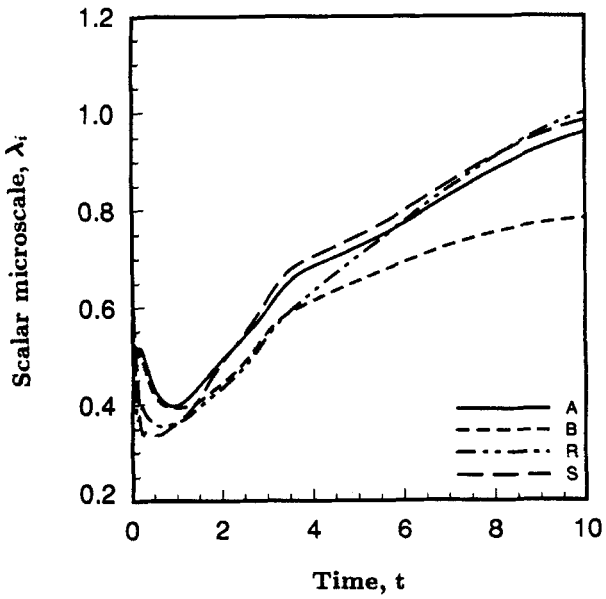

Figure 18. Evolution of scalar concentration microscales for case A and a blob initial scalar field.

Concentration microscales for inert species and reacting species have been discussed by Leonard and Hill (1991). Since reaction increases concentration gradients, the growth of the concentration microscales was found to be somewhat less when chemical reaction is present compared to the case with no reaction, although the difference was small. The growth rate of the concentration microscales was greater for an isotropic scalar field than for an anisotropic scalar field (Leonard and Hill, 1991). The evolution of concentration microscales for reactants and products are shown in Figure 17 for the slab case and in Figure 18 for the blob case, for simulations with a series-parallel reaction pair. Table 6 compares values of the nondimensional scalar microscale for the blob and slab initial scalar fields. Figure 19 shows that the growth of the concentration microscales is pronounced for the blob case and remains almost constant for the slab case, in agreement with the observations of Leonard and Hill (1991) for a single reaction.

Conclusions

Direct numerical simulations of the nonlinear dynamical equations have been performed to study the problem of chemical selectivity using a pseudo-spectral method on grids of 64^3 Fourier modes. Simulations were carried out in decaying, isotropic turbulence with varying R_λ and with initially segregated reactant species.

The effect of various physical parameters on selectivity was examined. Comparisons with the case of no velocity show that the presence of turbulence favors formation of the desired product R over the undesired product S. As the turbulence

Reynolds number is increased, mixing is enhanced and the formation of R is favored. A decrease in viscosity decreases the size of the small-scale structure of the velocity and scalar fields, thus favoring the formation of primary product R. A decrease in Sc at fixed R_λ implies an increase of diffusivity and favors the first reaction over the second. As the ratio of the rate constants (k_1/k_2) is increased, more of R is formed compared to S, because the relative rate of the two reactions determines the product distribution. When the initial stoichiometric amount of A is more than 0.5 times the initial stoichiometric amount of B, the formation of S is suppressed because the limiting reagent B gets exhausted and the second reaction cannot take place. Simulations for the case where the initial scalar field is isotropic show that the amount of R formed is considerably higher than for the case with a slab initial scalar field. The isotropic scalar field is three-dimensional and hence more homogenous, and thus transport is better compared to the slab scalar field where the transport is initially one-dimensional.

Comparisons of the local reaction rates for the one and two reaction cases were made. The reaction zones for the first and second reaction in the complex chemistry case do not coincide, as it appears that the reaction zone for the second reaction migrates towards the B-rich region. Examination of the spatial distribution of reaction rate for various values of physical parameters reveals the following details about the structure of the concentration field: (a) the scalar field is more detailed for a lower value of viscosity since more small-scale structures are present, and (b) the sizes of the scalar field structures decrease with an increase of diffusivity. Good mixing and homogeneity in A and R favored the formation of the intermediate R, and thus the effect of all the physical parameters can be explained in terms of the part played by the parameters in bringing about homogenization.

Acknowledgments

We gratefully acknowledge the computer resources provided by the National Center for Supercomputing Applications. Dr. R. M. Kerr is with the National Center for Atmospheric Research which is funded by the National Science Foundation. We also thank Prof. R. S. Brodkey for making some computer runs at the Ohio Supercomputer Center.

Notation

a, b = constants in initial energy spectrum
c_i = fluctuating component of concentration of species i
c_i' = root-mean-square value of concentration fluctuations of species i
$\overline{c_i c_j}$ = covariance of concentration fluctuations of species i and j
C = Courant number, as defined in Eq. 10
C_{i0} = initial concentration of species i
$\overline{C_i}$ = average concentration of species i
DNS = direct numerical simulation
Da_1 = Damköhler number for the first reaction $= k_1\sqrt{C_{A0}C_{B0}}\,\Lambda_f/u'$
Da_2 = Damköhler number for the second reaction $= k_2\sqrt{C_{A0}C_{B0}}\,\Lambda_f/u'$
D_{aI}, D_{aII} = Damköhler number of the first and second kind (Table 3)
$E(k, 0)$ = initial energy spectrum for the velocity field
$E_\phi(k, 0)$ = scalar test field
I_s = intensity of segregation $= -\overline{c_i c_j}/\overline{C}_i\overline{C}_j$
k = wavenumber vector
k_0 = peak wavenumber
k_1, k_2 = kinetic rate constants for the first and second reactions
L = length of spatial domain ($= 2\pi$ in arbitrary units)
N = number of Fourier modes in each direction
p = pressure
R_λ = turbulence Reynolds number, $u'\lambda_g/\nu$
t = time
t^* = presimulation diffusion time to eliminate Gibb's ringing
$\boldsymbol{u}$ = velocity
u' = turbulence intensity, $\sqrt{\overline{u_i u_i}/3}$
x, y, z = spatial coordinates
x', y' = spatial grid point location (Nx/L, Ny/L)
X_S = selectivity, as given in Eq. 2

Greek letters

α = constant
γ_{ij} = correlation coefficient between concentration fluctuations of species i and $j = \overline{c_i c_j}/c_i' c_j'$
Δt = time-step
η = Kolmogorov length scale
λ_g = Taylor microscale
λ_i = scalar microscale of species i
λ_{i0} = initial scalar microscale of species i
Λ_f = longitudinal integral length scale of the velocity field
ν = kinematic viscosity
ρ = density of the fluid
ω = vorticity

Specific symbols

$\hat{}$ = Fourier transformed variable
$\bar{}$ = time- or volume-averaged value

Literature Cited

Angst, W., J. R. Bourne, and R. N. Sharma, "Mixing and Fast Chemical Reaction: V. Influence of Diffusion within the Reaction Zone on Selectivity," *Chem. Eng. Sci.*, **37**, 1259 (1982).

Baldyga, J., and J. R. Bourne, "A Fluid Mechanical Approach to Turbulent Mixing and Chemical Reaction: I. Inadequacies of Available Methods," *Chem. Eng. Commun.*, **28**, 231 (1984a).

Baldyga, J., and J. R. Bourne, "A Fluid Mechanical Approach to Turbulent Mixing and Chemical Reaction: II. Micromixing in the Light of Turbulence Theory," *Chem. Eng. Commun.*, **28**, 243 (1984b).

Baldyga, J., and J. R. Bourne, "A Fluid Mechanical Approach to Turbulent Mixing and Chemical Reaction: III. Computational and Experimental Results for the New Micromixing Model," *Chem. Eng. Commun.*, **28**, 259 (1984c).

Baldyga, J., and J. R. Bourne, "Simplification of Micromixing Calculations: I. Derivation and Application of New Model," *Chem. Eng. J.*, **42**, 83 (1989a).

Baldyga, J., and J. R. Bourne, "Simplification of Micromixing Calculations: II. New Applications," *Chem. Eng. J.*, **42**, 83 (1989b).

Bird, R. B., W. E. Stewart, and E. N. Lightfoot, *Transport Phenomena*, Wiley, New York, p. 557 (1960).

Bourne, J. R., "Characterization of Micromixing Using Fast Multiple Reactions," *Chem. Eng. Commun.*, **16**, 79 (1982).

Bourne, J. R., F. Kozicki, and P. Rys, "Mixing and Fast Chemical Reaction: I. Test Reactions to Determine Segregation," *Chem. Eng. Sci.*, **36**, 1643 (1981).

Bourne, J. R., U. Moergeli, and P. Rys, "Mixing and Fast Chemical Reaction: Influence of Viscosity on Product Distribution," *Proc. Euro. Conf. on Mixing*, BHRA, Fluid Engineering Center, Cranfield, U.K., p. B3 (1978).

Bourne, J. R., and H. L. Toor, "Simple Criteria for Mixing Effects in Complex Reactions," *AIChE J.*, **23**, 602 (1977).

Chakrabarti, M., and J. C. Hill, "Direct Numerical Simulation of a Parallel-consecutive Reaction Pair in Homogenous Turbulence," *Proc. Symp. on Turbulence*, Rolla, MO (1990).

Chakrabarti, M., "Numerical Studies of Chemical Selectivity and Heat Transfer in Decaying Homogenous Turbulence," PhD Diss., Iowa State Univ., Ames (1991).

Chakrabarti, M., and J. C. Hill, "Tests of First Order Closure Theories for a Series-Parallel Reaction in a Simulated Homogeneous Turbulence," AIChE Meeting, Miami Beach, FL (1995).
Cheng, D. C. H., and D. J. Tookey, "The Effect of Agitator Geometry and Speed on Yield in Batch Reactors," *Proc. Euro. Conf. on Mixing*, BHRA, Fluid Engineering Center, Cranfield, U.K., p. A1-1 (1978).
Danckwerts, P. V., "The Definition and Measurement of Some Characteristics of Mixtures," *Appl. Sci. Res.*, **3**, 279 (1952).
Gao, F., and E. E. O'Brien, "Direct Numerical Simulations of Reacting Flows in Homogenous Turbulence," *AIChE J.*, **37**, 1459 (1991).
Givi, P., and P. A. McMurtry, "Non-Premixed Reaction in Homogenous Turbulence: Direct Numerical Simulations," *AIChE J.*, **34**, 1039 (1988).
Heeb, T. G., "Examination of Turbulent Mixing with Multiple Second-order Chemical Reactions by the Statistical Analysis Technique," PhD Diss., Ohio State Univ., Columbus (1986).
Hill, J. C., "Homogenous Turbulent Mixing with Chemical Reaction," *Ann. Rev. Fluid Mech.*, **8**, 135 (1976).
Hinze, J. O., *Turbulence*, 2nd ed., McGraw Hill, New York (1975).
Kerr, R. M., "Higher-Order Derivative Correlations and the Alignment of Small-Scale Structures in Isotropic Numerical Turbulence," *J. Fluid Mech.*, **153**, 31 (1985).
Leonard, A. D., "Direct Numerical Simulations of Chemically Reacting Turbulence Flows," PhD Diss., Iowa State Univ., Ames (1989).
Leonard, A. D., and J. C. Hill, "Direct Numerical Simulation of Turbulent Flows with Chemical Reaction," *J. Sci. Computing*, **3**, 25 (1988).
Leonard, A. D., and J. C. Hill, "Direct Numerical Simulation and Simple Closure Theory for a Chemical Reaction in Homogenous Turbulence," *Turbulent Reactive Flows*, R. Borghi and S. N. B. Murthy, eds., Lecture Notes in Engineering, **40**, Springer-Verlag, New York, 515 (1989).
Leonard, A. D., and J. C. Hill, "Scalar Dissipation and Mixing Turbulent Reacting Flows," *Phys. Fluids A*, **3**, 1286 (1991).
Levenspiel, O., *Chemical Reaction Engineering*, 2nd ed., Wiley, New York, p. 343 (1972).
Li, K. T., and H. L. Toor, "Turbulent Reactive Mixing with a Series-Parallel Reaction: Effect of Mixing on Yield," *AIChE J.*, **32**, 1312 (1986).
Mao, K. W., and H. L. Toor, "Second-Order Chemical Reactions with Turbulent Mixing," *Ind. Eng. Chem. Fund.*, **10**, 192 (1971).
Mehta, R. V., and J. M. Tarbell, "Four Environment Model of Mixing and Chemical Reaction: I. Model Development," *AIChE J.*, **29**, 320 (1983).
Mehta, R. V., and J. M. Tarbell, "An Experimental Study of the Effect of Turbulent Mixing on the Selectivity of Competing Reactions," *AIChE J.*, **33**, 1089 (1987).
Mell, W. E., V. Nilsen, G. Kosaly, and J. J. Riley, "Direct Numerical Simulation Investigation of the Conditional Moment Closure Model for Nonpremixed Turbulent Reacting Flows," *Combust. Sci. and Tech.*, **91**, 179 (1993).
Nauman, E. B., "The Droplet Diffusion Model for Micromixing," *Chem. Eng. Sci.*, **30**, 1135 (1975).
Oran, E. S., and J. P. Boris, *Numerical Simulation of Reactive Flow*, Elsevier, New York (1987).
Orszag, S. A., "Numerical Simulation of Incompressible Flows within Simple Boundaries. I. Galerkin (spectral) Representations," *Studies Appl. Math.*, **50**, 293 (1971).
Patterson, G. K., "Modelling of Turbulent Reactors," *Mixing of Liquids by Mechanical Agitation*, Jaromir J. Ulbrecht and Gary K. Patterson, eds., Gordon and Breach Science Publishers, New York, p. 59 (1985).
Paul, E. L., and R. E. Treybal, "Mixing and Product-Distribution for a Liquid-Phase, Second-Order, Competitive-Consecutive Reaction," *AIChE J.*, **17**, 718 (1971).
Pfister, F., P. Rys, and H. Zollinger, "Chemical Selectivities Disguised by Mass Diffusion: II. Mixing-Disguised Nitrations of Aromatic Compounds with Nitronium Salts," *Helvetica Chimica Acta*, **58**, 2094 (1975).
Tarbell, J. M., and R. V. Mehta, "Mechanistic Models of Mixing and Chemical Reaction with a Turbulence Analogy," *Physicochem. Hydrodyn.*, **7**, 17 (1986).

Manuscript received July 21, 1994, and revision received Dec. 16, 1994.